

Collapse of the Pseudogap in Cuprate Superconductors at a Lifshitz Transition

S. Benhabib¹, A. Sacuto¹, M. Civelli², I. Paul¹, M. Cazayous¹, Y. Gallais¹, M.-A. Méasson¹, R. D. Zhong³, J. Schneeloch³ and G. D. Gu³, D. Colson⁴ and A. Forget⁴

¹ *Laboratoire Matériaux et Phénomènes Quantiques (UMR 7162 CNRS),*

Université Paris Diderot-Paris 7, Bat. Condorcet, 75205 Paris Cedex 13, France,

² *Laboratoire de Physique des Solides, (UMR 8502 CNRS),*

Université Paris Sud, Bat.510, 91405 Orsay Cedex,

³ *Matter Physics and Materials Science, Brookhaven National Laboratory (BNL), Upton, NY 11973, USA,*

⁴ *Service de Physique de l'Etat Condensé, CEA-Saclay, 91191 Gif-sur-Yvette, France*

(Dated: December 3, 2024)

The puzzling pseudogap phase of the cuprates poses one of the greatest challenges for understanding high-temperature superconductivity [1]. Although intensely studied in the underdoped regime [2, 3], relatively less is known about the pseudogap on the overdoped side, where it weakens and eventually disappears at a critical doping p_c [4]. Here, combining Raman spectroscopy on $\text{Bi}_2\text{Sr}_2\text{CaCu}_2\text{O}_{8+\delta}$ (Bi-2212) over a large range of finely tuned doping with theoretical calculations, we determine $p_c = 0.22$, and we reveal that it coincides with a Lifshitz transition where the underlying hole-like active Fermi surface becomes electron-like at a van Hove singularity. Interestingly, the superconducting critical temperature T_c is unaffected by this transition. Comparing our results with existing photoemission and tunnelling data, we demonstrate that the microscopic origins of the pseudogap and the superconductivity are different on the overdoped side. Only the former is tied to the change in the Fermi surface topology, a feature universal across several hole doped cuprates.

The depletion of low energy electronic excitations, described as the pseudogap feature below T^* , is a defining characteristic of the cuprate high-transition-temperature (high T_c) superconductors [2]. Much of current research on this subject is dominated by the quest to understand its microscopic origin, and how it is related to the superconducting phase [5]. This feature is strongest at low hole doping p , where the cuprates are doped Mott insulators, and it weakens with increasing p . Thus, one logical line of enquiry is to determine the critical doping p_c where the pseudogap closes, and to identify what triggers it in the first place. Significantly, few recent works, such as a transport study of $\text{La}_{1.6-x}\text{Nd}_{0.4}\text{Sr}_x\text{CuO}_4$ [6] and an angle-resolved photo-emission spectroscopy (ARPES) on Bi-2212 [7] have inferred quantum phase transition associated with the pseudogap closing. Clearly, at this point, identifying the nature of this transition constitutes an important step forward.

One technical obstacle to address the above issue is the lack of sufficiently overdoped samples belonging to the same family of cuprates. Indeed, the current work was made possible due to the availability of high qual-

ity Bi-2212 single crystals, several of which with doping close to $p_c = 0.22$ (see experimental procedure and supplementary information, SI). This allowed for a careful finely tuned study of the doping dependence around the critical value. The level of doping was controlled only by oxygen insertion, and the highest level of doping achieved was around $p = 0.24$. The Raman measurements were performed in $\nu = B_{1g}, B_{2g}$ geometries that probe respectively the antinodal (AN) region near $(\pm\pi, 0)$ and $(0, \pm\pi)$ and the nodal (N) region near $(\pm\pi, \pm\pi)$ and $(\pm\pi, \pm\pi)$, (see experimental procedure).

In Fig. 1 we show representative $\chi''_{B_{1g}}(\omega)$ (red/grey) and $\chi''_{B_{2g}}(\omega)$ (black) Raman responses, at 10 K (superconducting state) and at 110 K (normal state) for selected doping levels. The Raman shift is expressed in units of Δ_0 , the superconducting gap, in order to compare better samples with varying $\Delta_0(p)$. Here, we concentrate on the broad electronic background, ignoring the sharp phonon peaks [8] (at $0.3 \Delta_0(p)$ and $\Delta_0(p)$ in top left panel). We note that the integrated area of the normal and superconducting B_{1g} responses are less than those of the B_{2g} responses at low doping, but the situation is reversed in the vicinity of the optimal doping level $p = 0.16$. Indeed, we observe that the B_{1g} response increases continuously in magnitude compared to the B_{2g} response for $p \leq 0.22$, consistent with earlier studies [9–15]. However, beyond 0.22 doping the trend changes and require more careful analysis.

Crucially, from the Raman responses $\chi''_\nu(\omega)$, (of which representative ones are displayed in Fig.1) we extract and report in Fig. 2(a) the ratio $I_{B_{1g}}/I_{B_{2g}}$ of the integrated intensities defined by

$$I_\nu(T) = \int_0^\Lambda d\omega \chi''_\nu(\omega, T). \quad (1)$$

In our analysis we set the cutoff $\Lambda \approx 3\Delta_0$, and we checked that varying Λ does not change the results. Studying the intensity ratio rather than the absolute intensities of the Raman response, allowed us to prevent from some non intrinsic intensity modulations when passing from one crystal to another (see experimental procedure). The intensity ratios in the superconducting (filled circles) and the normal states (open circles) are nearly the same, thereby indicating that $I_{B_{1g}}/I_{B_{2g}}$ is unaffected by the superconducting gap. Based on its doping depen-

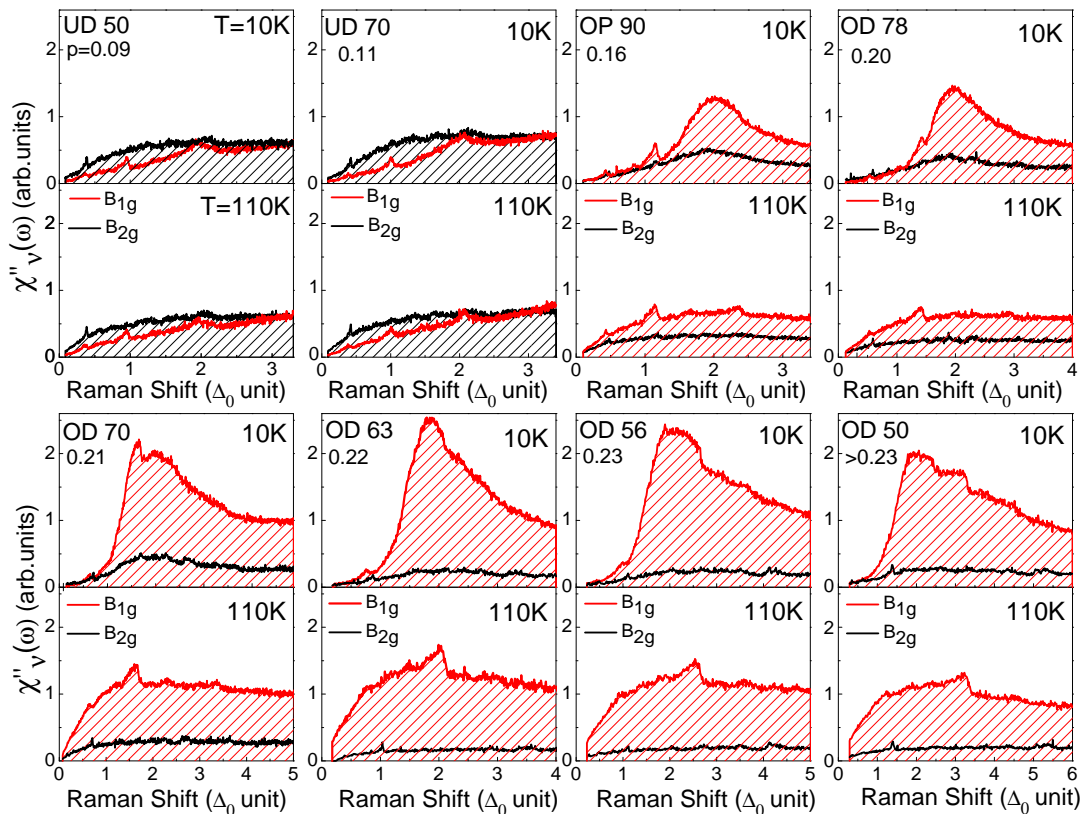


FIG. 1. B_{1g} (red/grey) and B_{2g} (black) Raman responses of Bi-2212 at 10 K and 110 K for selected doping levels. The magnitude of the B_{1g} response increases in comparison to the B_{2g} one as a function of doping up to $p = 0.22$. The black hatched area signal a larger magnitude of the B_{2g} response with respect to the B_{1g} one and the (red/grey) hatched area shows the oposite. The 532 nm laser line was used. The Raman shift is expressed in units of the superconducting gap Δ_0 defined from the position of the B_{1g} pair breaking peak (see SI). T_c was estimated from susceptibility measurements (see experimental procedure). We found a remarkably linear dependence between T_c and Δ_0 for the overdoped regime and the doping level for each value of T_c was fixed using the Tallon-Presland formula (see SI).

dence we identify three distinct regimes. (i) a regime of moderate increase for $0.08 < p < 0.13$.

(ii) $0.13 < p < 0.20$, over which the intensity ratio is nearly constant. (iii) Most importantly, for $p > 0.20$ the ratio increases dramatically, and reveals a well defined sharp peak located at $p = 0.22$.

We confirmed that the sharp peak is not a resonance effect, since it is visible with two distinct laser lines, namely 532 nm and 647.1 nm. An earlier Raman measurement did not detect any significant resonance either [16].

Now, we establish that the location of the sharp peak coincides with the critical doping p_c where the normal state pseudogap closes. To this purpose, we first show in Fig. 2(b) the doping evolution of the subtracted spectra $\chi''_{B_{1g}}(\omega, T_c) - \chi''_{B_{1g}}(\omega, T^*)$, where the pseudogap depletion appears as the white negative unshaded area. T^* was obtained from the temperature dependence of the B_{1g} spectra (reported in SI). We see that the pseudogap depletion shrinks with the increase of doping, and disappears at $p = 0.22$ beyond which only a positive low energy electronic background is detected. Secondly, we define the integrated intensity of the pseudogap depletion

as $I_{B_{1g}}(T_c) - I_{B_{1g}}(T^*)$, and we plot its doping evolution (filled stars) in Fig. 2(a), which clearly shows a decrease with doping and the pseudogap closing at $p_c = 0.22$ where $I_{B_{1g}}/I_{B_{2g}}$ is peaked.

Note that the peak in $I_{B_{1g}}/I_{B_{2g}}$ cannot be attributed to the doping dependence of the pseudogap which is monotonic. Instead, the temperature independence of the sharp peak position indicates that it is related to enhanced density of states of the underlying band structure around the AN region of the Brillouin zone (see Fig. 3(b,c)). This invariably leads to the possibility of a doping induced Lifshitz transition wherein, as a van Hove singularity crosses the Fermi in the AN region, the open hole-like anti-bonding Fermi surface becomes electron-like.

An electron-like anti-bonding band in Bi-2212 at $p > 0.22$ has been reported by ARPES data [17], and can be relevant as well to understand the anomalous peak reported by muon-spin rotation on overdoped cuprates [18, 19].

In order to support this scenario we perform theoretical calculation of the Raman response function using a

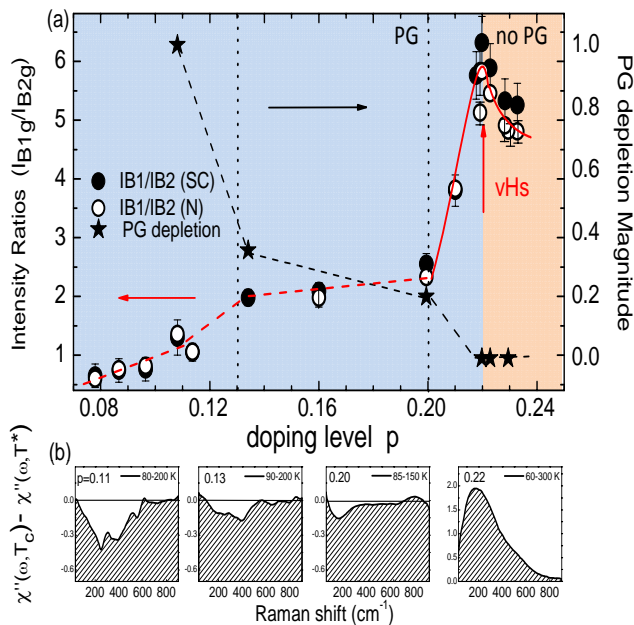


FIG. 2. (a) Doping evolution of (i) the ratio $I_{B_{1g}}/I_{B_{2g}}$ of the integrated intensity (defined in eq. 1) in the superconducting and the normal states (filled and open circles respectively), (ii) the pseudogap depletion (black star). We distinguish three regimes that are marked by vertical dotted lines in the doping phase diagram. The peak in the ratio $I_{B_{1g}}/I_{B_{2g}}$, both for the superconducting and the normal phases, coincides with the critical doping $p_c = 0.22$ where the pseudogap vanishes. (b) Spectral depletion due to the pseudogap (white negative unshaded area) obtained by subtracting the B_{1g} Raman response just above T_c from that close to T^* (for details, see SI). The pseudogap decreases with increasing doping p and disappears at p_c .

minimal tight-binding model for a bilayer cuprate with the normal state dispersion [20]: $\epsilon_{k,\alpha} = -2t(\cos k_x + \cos k_y) + 4t' \cos k_x \cos k_y \pm t_o (\cos k_x - \cos k_y)^2/4 - \mu$. Here $\alpha = \pm$ refer to the anti-bonding (AB) and the bonding (B) bands. The superconducting dispersion is given by $E_k = \sqrt{\epsilon_k^2 + \Delta_k^2}$, with $\Delta_k = \Delta_0(\cos k_x - \cos k_y)/2$. We take $t' = -0.3t$, $t_o = 0.084t$, and a doping independent $\Delta_0 = 0.0025t$. We change p by varying the chemical potential μ . As shown in Fig. 3(b)-(d), this model undergoes a Lifshitz transition at $p = 0.22$ where the AB band changes from being hole- to electron-like (the B band remains hole-like in this doping range, see SI). We take a constant electron scattering rate $\Gamma_N = 0.01t$ and $\Gamma_S = 0.0025t$ in the normal and the superconducting states respectively. The calculation of $\chi''_{\nu}(\omega)$ and I_{ν} are standard (for details, see SI). The doping dependence of the calculated ratio $I_{B_{1g}}/I_{B_{2g}}$ shows prominent peaks at $p = 0.22$ (Fig. 3(a)), both in the normal and the superconducting states, and reproduces qualitatively the experimental trend in the third regime of Fig. 2(a).

The origin of the peak can be captured conveniently by tracking the doping dependence of the Raman vertex $\gamma''_{k,\alpha}$ -weighted density of states $N_{\nu}(\omega) \equiv$

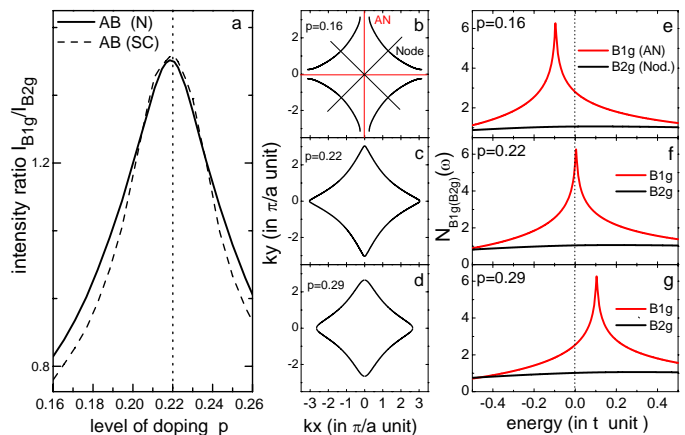


FIG. 3. (a) Doping dependence of the integrated intensity ratio $I_{B_{1g}}/I_{B_{2g}}$ in the normal (solid line) and superconducting (dashed line) states calculated from a theoretical model (see text). The curves have been normalized (see SI). The results are in qualitative agreement with the data of Fig. 2(a). The peaks are due to a Lifshitz transition (see (b)-(d)). (b)-(d) Doping dependence of the anti-bonding Fermi surface. From hole-like it becomes electron-like at a Lifshitz transition. (e)-(g) The associated van Hove singularity (which develops in the AN region) appears in $N_{B_{1g}}(\omega)$ (red/grey), the density of states weighted by the B_{1g} Raman vertex (defined in text), but not in $N_{B_{2g}}(\omega)$ (black). Consequently, the theoretical $I_{B_{2g}}$ is nearly doping independent, while $I_{B_{1g}}$ is maximum at the doping where the van Hove singularity crosses the chemical potential. This gives the peaks in panel (a). $N_{B_{2g}}(\omega)$ is multipled by $(t/t')^2$ for better visibility.

$\sum_{k,\alpha} (\gamma''_{k,\alpha})^2 \delta(\omega - \epsilon_{k,\alpha})$ which enter the calculation of I_{ν} . As shown in Fig. 3(e)-(g), the van Hove singularity shows up in $N_{B_{1g}}(\omega)$, and the peak in the intensity $I_{B_{1g}}$ corresponds to the van Hove singularity crossing the chemical potential. Simultaneously, since the B_{2g} geometry probes the diagonal directions of the Brillouin zone, $N_{B_{2g}}(\omega)$ is unaffected by the van Hove singularity and therefore $I_{B_{2g}}$ has no significant doping dependence.

In principle, the scenario above does not preclude the possibility that for $p > 0.22$ the pseudogap exists in the hole-like B band. However, we do not find any signature of it in the Raman spectra, consistent with ARPES results [7]. One possibility is that the response is predominantly from the AB band since it is close to a density of states singularity. We notice this trend in the theoretical calculation as well (see SI).

Now, we comment upon the universality of our findings. An intriguing pattern emerges upon comparing our results with the existing literature on other hole doped cuprate families near the critical doping p_c (Fig. 4). In contrast with Bi-2212 and $\text{La}_{1.6-x}\text{Nd}_{0.4}\text{Sr}_x\text{CuO}_4$ [6], where p_c is located inside the superconducting dome, in ARPES measurements on $\text{La}_{2-x}\text{Sr}_x\text{CuO}_4$ (LSCO) [21] the pseudogap and the superconducting phases appear to end at the same doping. Scanning tunneling spectroscopy on $\text{Bi}_2\text{Sr}_2\text{CuO}_{6+\delta}$ (Bi-2201) instead, found the pseudogap extending well into the normal phase [22]. This

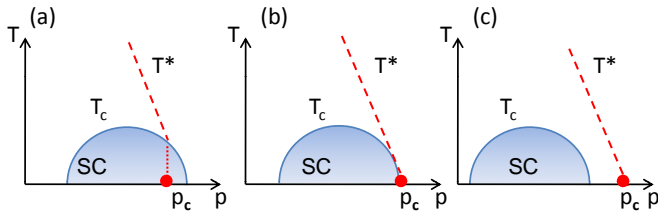


FIG. 4. Schematic temperature (T) versus doping (p) phase diagram with three material-dependent possible locations of the critical doping p_c , where the normal state pseudogap closes, with respect to the superconducting (SC) dome (shaded blue/grey). (a) is realized in Bi-2212 (current study), (b) and (c) have been reported for LSCO and Bi-2201 respectively. The universal feature in all three cases is the coincidence of p_c with a Lifshitz transition where a Fermi surface changes from hole-like to electron-like.

suggests that the location of p_c with respect to the superconducting dome is material dependent (see Fig. 4). However, interestingly, just as we established here for Bi-2212, for both LSCO and Bi-2201 data analyses have suggested the coincidence of the pseudogap closing with a Lifshitz transition. Taken together, this appears to be a universal feature of the hole doped cuprates, and our findings provide the missing piece that establishes an intimate connection between the pseudogap and Fermi surface topology. We also note that, a Lifshitz transition in overdoped $Tl_2Ba_2CuO_{6+\delta}$, (Tl-2201) is yet to be reported, but strong enhancement of antinodal ARPES intensity, indicative of proximity to a van Hove singularity, has been observed [23].

The above conclusions have far-reaching consequences for the theory of high temperature superconductivity in the cuprates. Our results show that, on the overdoped side of the cuprates, the microscopic origins of the pseudogap and the superconductivity are different. It also emphasizes the importance of interplay between the Fermi surface topology and the pseudogap mechanism. This is in agreement with theoretical works that find interaction effects to diminish in the antinodal region when a hole-like Fermi surface becomes electron-like [24–27].

EXPERIMENTAL PROCEDURE

Raman Experiments

Raman experiments have been carried out using a triple grating spectrometer (JY-T64000) equipped with a liquid-nitrogen-cooled CCD detector. Two laser excitation lines were used: 532 nm and 647.1 nm from respectively a diode pump solid state laser and a Ar+/Kr+ mixed laser gas. The B_{1g} and B_{2g} geometries have been obtained from cross polarizations at 45° from the Cu-O bond directions and along them respectively. The

change from B_{1g} to B_{2g} geometries was obtained by keeping fixed the orientations of the analyzers and the polarizers fixed and by rotating the crystal using an Attocube piezo-driven rotator. We got an accuracy on the crystallographic axes orientation with respect to the polarizers close to 2° . Importantly, we succeeded in measuring the B_{1g} and B_{2g} Raman responses of each crystal on the same laser spot. This allowed us to keep constant the solid angle of collection and made reliable the B_{1g} to B_{2g} Raman intensity ratio.

All the spectra have been corrected for the Bose factor, the instrumental spectral response. They are thus proportional to the imaginary part of the Raman response function $\chi''_r(\omega)$. Measurements between 4 and 300 K have been performed using an ARS closed-cycle He cryostat. The laser power at the entrance of cryostat was maintained below 2 mW to avoid over heating of the crystal estimated to 3 K/mW at 10 K.

Crystal Growth and Characterization

The Bi-2212 single crystals were grown by using a floating zone method. The optimal doped sample with $T_c = 90$ K was grown at a velocity of 0.2 mm per hour in air [28]. In order to get overdoped samples down to $T_c = 65$ K, the as-grown single crystal was put into a high oxygen pressured cell between 1000 and 2000 bars and then was annealed from $350^\circ C$ to $500^\circ C$ during 3 days [29]. In order to get the underdoped sample down to $T_c = 50$ K, the optimal doping crystal was annealed between $350^\circ C$ and $550^\circ C$ during 3 days under vacuum of $1.3 \cdot 10^{-6}$ mbar. Finally, the overdoped samples below $T_c = 60$ K was obtained from as-grown Bi-2212 single crystals put into a pressure cell (Autoclave France) with 100 bars oxygen pressure and then annealed from 4 to 7 days at $350^\circ C$ or 5 days at $350^\circ C$ then 5 days at $350^\circ C$. Then the samples were rapidly cooled to room temperature by maintaining a pressure of 100 bars. The critical temperature T_c for each crystal has been determined from magnetization susceptibility measurements at a 10 Gauss field parallel to the c-axis of the crystal. More than 30 crystals have been measured among 60 tested. The selected crystals exhibit a quality factor of $T_c/\Delta T_c$ larger than 7. ΔT_c is the full width of T_c transition measured. A complementary estimate of T_c was achieved from electronic Raman scattering measurements by defining the temperature from which the B_{1g} superconducting pair breaking peak collapses.

ACKNOWLEDGEMENTS

We are grateful to A. Georges for very helpful discussions. Correspondences and requests for materials should be addressed to A.S (alain.sacuto@univ-paris-diderot.fr)

-
- [1] Norman, M. R., Pines, D. & Kallin, C. The pseudogap: friend or foe of high Tc? *Adv. Phys.* **54**, 712 (2005).
- [2] Timusk, T. & Statt, B. The pseudogap in high-temperature superconductors: an experimental survey. *Rep. Prog. Phys.* **62** 122(1999).
- [3] Hussey, N. E. Phenomenology of the normal state in-plane transport properties of high-Tc cuprates. *J. Phys. : Condens. Matter* **20** 123201 (2008).
- [4] Tallon, J. L. & Loram, J.W. The doping dependence of T^* , what is the real high-Tc phase diagram? *Physica C* **349**, 53 (2001).
- [5] Lee, P. A., Nagaosa, N., & Wen, X-G., Doping a Mott insulator: physics of high-temperature superconductivity. *Rev. Mod. Phys.* **78**, 17 (2006).
- [6] Daou, R. *et al.* Linear temperature dependence of resistivity and change in the Fermi surface at the pseudogap critical point of a high-Tc superconductor *Nature Physics* **5**, 31 (2009).
- [7] Vishik, I. M. *et al.* Phase competition in trisected superconducting dome. *PNAS* **109**, 18332 (2012).
- [8] Kakihana, M. *et al.* Raman-active phonons in $\text{Bi}_2\text{Sr}_2\text{Ca}_{1-x}\text{Y}_x\text{Cu}_2\text{O}_{8+d}$ ($x=0.1$): Effects of hole filling and internal pressure induced by Y doping for Ca, and implications for phonon assignments. *Phys. Rev. B* **53** 11796 (1996).
- [9] Blanc, S. *et al.*, Quantitative Raman measurement of the evolution of the Cooper-pair density with doping in $\text{Bi}_2\text{Sr}_2\text{CaCu}_2\text{O}_{8+\delta}$ superconductors. *Phys. Rev. B* **80**, 140502R (2009).
- [10] Hewitt, K. C. & Irwin, J. C. Doping dependence of the superconducting gap in $\text{Bi}_2\text{Sr}_2\text{CaCu}_2\text{O}_{8+\delta}$. *Phys. Rev. B* **66**, 054516 (2002).
- [11] Prestel, W. *et al.* Pair breaking versus symmetry breaking: Origin of the Raman modes in superconducting cuprates. *Phys. Rev. B* **84**, 144523 (2011).
- [12] Munnikes, N. Pair breaking versus symmetry breaking: origin of the Raman modes in superconducting cuprates. *Phys. Rev. B* **84**, 144523 (2011).
- [13] Masui, T. *et al.* Raman study of carrier-overdoping effects on the gap in high-Tc superconducting cuprates. *Phys. Rev. B* **68**, 060506(R) (2003); Masui, T. *et al.* Electronic crossover in the overdoped high-temperature (Y,Ca) $\text{Ba}_2\text{Cu}_3\text{O}_y$ superconductor by Raman scattering. *et al. Phys. Rev. B* **79**, 014511 (2009).
- [14] Naeini, J. G. *et al.* Doping dependence of the pseudogap in $\text{La}_{2-x}\text{Sr}_x\text{CuO}_4$. *Phys. Rev. B* **59**, 9642 (1999).
- [15] Gasparov, L. V., Lemmens, P., Kolesnikov, N.N. & Guntherodt, G. Electronic Raman scattering in $\text{Tl}_2\text{Ba}_2\text{CuO}_{6+\delta}$: Symmetry of the order parameter, oxygen doping effects, and normal-state scattering. *Phys. Rev. B* **58**, 11753, (1998).
- [16] Venturini, F. *et al.* Observation of an Unconventional Metal-Insulator Transition in Overdoped CuO_2 Compounds. *Phys. Rev. Lett.* **89**, 107003 (2002).
- [17] A. Kaminski, *et al.* Change of Fermi-surface topology in $\text{Bi}_2\text{Sr}_2\text{CaCu}_2\text{O}_{8+\delta}$ with doping *Phys. Rev. B* **73**, 174511 (2006).
- [18] Bernhard, C., Tallon, J. L., Blasius, Th., Golnik, A. & Niedermayer, Ch. Anomalous Peak in the Superconducting Condensate Density of Cuprate High-Tc Superconductors at a Unique Doping State. *Phys. Rev. Lett.* **86**, 1614 (2001).
- [19] Uemura, Y. J. *et al.*, Universal Correlations between Tc and ns/m^* ? (carrier density over effective mass) in high-Tc cuprate Superconductors. *Phys. Rev. Lett.* **62**, 2317 (1989).
- [20] Kordyuk, A. A., Borisenko, S. V., Knupfer, M. & Fink, J. Measuring the gap in angle-resolved photoemission experiments on cuprates. *Phys. Rev. B* **67**, 064504 (2003).
- [21] Ino, A. Doping dependent evolution of the electronic structure of $\text{La}_{2-x}\text{Sr}_x\text{CuO}_4$ in the superconducting and metallic phases. *Phys. Rev. B* **65**, 094504 (2002).
- [22] Piriou, A., Jenkins, N., Berthod, C., Maggio-Aprile, I. & Fisher, O. First direct observation of the van Hove singularity in the tunnelling spectra of cuprates. *ncomms* **1229** (2011).
- [23] Platé, M. Anomalous Momentum dependence of the quasiparticle scattering rate in overdoped $\text{Bi}_2\text{Sr}_2\text{CaCu}_2\text{O}_8$. *et al. Phys. Rev. Lett.* **95**, 0077001, (2005).
- [24] Civelli, M., Capone, M., Kancharla, S. S., Parcollet, O., & Kotliar, G. Dynamical Breakup of the Fermi Surface in a Doped Mott Insulator. *Phys. Rev. Lett.* **95**, 106402 (2005).
- [25] Kyung, B. Pseudogap induced by short-range spin correlations in a doped Mott insulator. *Phys. Rev. B* **73**, 165114 (2006).
- [26] Ferrero, M., Pseudogap opening and formation of Fermi arcs as an orbital-selective Mott transition in momentum space *Phys. Rev. B* **80**, 064501 (2009).
- [27] Sakai, S. *et al.* Raman-scattering measurements and theory of the energy-momentum spectrum for underdoped $\text{Bi}_2\text{Sr}_2\text{Ca}_{1-x}\text{Y}_x\text{Cu}_2\text{O}_{8+d}$ Superconductors: evidence of an s-Wave Structure for the Pseudogap. *Phys. Rev. Lett.* **111**, 107001 (2013).
- [28] Wen, J. S. Large Bi-2212 single crystal growth by the floating-zone technique. *J. of Crystal Growth* **310**, 1401 (2008).
- [29] Mihaly, L., Kendziora, C., Hartge, J., Mandrus, D. & Forro, L. High-pressure cell for oxygen annealing at elevated temperatures. *Rev. Sci. Instrum.* **64**, 2397 (1993).

SUPPLEMENTARY INFORMATIONS

A. Estimate of Δ_0 and its relationship to T_c

The determination of Δ_0 was achieved by subtracting the normal B_{1g} Raman response at 110 K from the B_{1g} one in the superconducting state at 10 K. We define $2\Delta_0$ as the maximum of the electronic background in the subtracted spectra, see Fig.5.

Special care has been devoted to select single crystals which exhibit the same $2\Delta_0$ value in the Raman spectra measured from distinct laser spots on a freshly cleaved surface. We find that T_c increases linearly with $2\Delta_0$ in the overdoped regime and reaches its maximum value at $T_c^{max} = 90$ K. From a linear fit of the T_c values, we find the reliable relationship: $T_c = (2\Delta_0)/8.2 + 28.6$ (1). In the underdoped regime T_c falls down abruptly as a function of $2\Delta_0$ (see Fig.6). The level of doping p was defined from T_c using Presland and Tallon's equation[1]: $1 - T_c/T_c^{max} = 82.6(p - 0.16)^2$ (2). In the overdoped regime, estimate of p can be directly determined from $2\Delta_0$ using both equations (1) and (2).

B. Estimate of T^* from Temperature dependence of the normal Raman response

In the left panel of Fig.7 is displayed, the temperature dependences of the B_{1g} Raman response of Bi-2212 single crystals for selected levels of doping. Notice that T_c and p values have been more accurately estimated compare to ref. [2] thanks to eq.(1) deduced from Fig.6. The thick (red/grey) and black curves correspond respectively to the spectra measured just above T_c and very close to T^* . T^* is the pseudogap temperature above which the electronic background is recovered. The temperature dependence of the normalized integrated area of the B_{1g} Raman response for selected doping levels is shown in the right panel of Fig.7. We have defined T^* as the temperature for which the integrated area is maximum, i.e. the temperature for which the low energy electronic background intensity is restored. Making the subtraction between the Raman spectra just above T_c and very close T^* allows us to point out the pseudogap depletion displayed in Fig. 2 (a) of the main text.

C. Theoretical Raman calculation

We calculate the electronic Raman response using standard zero-temperature linear response theory [3, 4]. This is given by

$$\chi''_{\nu}(\Omega) = \sum_{\alpha=AB,B} \int_{-\Omega}^0 \sum_k \gamma'_{k,\alpha} \text{Im}G_{\alpha}(k, i\omega) \text{Im}G_{\alpha}(k, i\omega + i\Omega) - \text{Im}F_{\alpha}(k, i\omega) \text{Im}F_{\alpha}(k, i\omega + i\Omega) \quad (1)$$

where the Raman vertex in the geometry $\nu = (B_{1g}, B_{2g})$ is $\gamma'_{k,\alpha} = \frac{m}{\hbar^2} \sum_{a,b} e_a^{I,\nu} \frac{\partial^2 \epsilon_a^{\alpha}}{\partial k_a \partial k_b} e_b^{S,\nu}$, with (a, b) denoting spatial directions (x, y) , e^I and e^S are polarization vectors for the incident and the scattered light respectively. The normal-state one particle propagator is given by $G(k, \omega) = 1/(\omega - \epsilon_k + i\Gamma_N)$, while in the superconducting state it can be written in a Nambu formalism:

$$\hat{G}(k, \omega) = \begin{pmatrix} G(k, \omega) & F(k, \omega) \\ F(k, \omega) & -G^*(k, -\omega) \end{pmatrix} = \begin{pmatrix} \omega - \epsilon_k + i\Gamma_S & \Delta_k \\ \Delta_k & \omega + \epsilon_k + i\Gamma_S \end{pmatrix}^{-1} \quad (2)$$

Here we have introduced a constant scattering rate $\Gamma_N = 0.01t$ and $\Gamma_S = 0.0025t$ in the normal and superconducting state respectively. In order to portray the superconducting state, we have introduced a d-wave superconducting gap $\Delta_k = (\Delta_0/2)(\cos k_x - \cos k_y)$, with $\Delta_0 = 0.025t$. Since our aim is to study only the effect of the Fermi surface topology change and the associated van Hove singularity on the Raman response, we do not change Δ_0 with the doping.

The Lifshitz transition in the AB band at the critical doping $p_c = 0.22$ is clearly visible in the B_{1g} Raman response, since in this geometry one probes mainly the antinodal parts of the Fermi surface close to the $k = (0, \pm\pi)$ and $(\pm\pi, 0)$. The Raman-vertex-weighted density of states $N_{B_{1g}}(\omega)$ (defined in the main text) presents in this case a singularity at the chemical potential (see Fig. 3.(f), main text), and therefore the $\chi''_{B_{1g}}(\omega)$ increases substantially and present a maximum at p_c , see top panels of Fig.8 (a) and (b). Instead, the $N_{B_{2g}}(\omega)$ does not present any singularity, since in this geometry one probes mainly the nodal regions of the Brillouin zone. Consequently the B_{2g} Raman response is not affected by the Lifshitz transition, and it displays little doping dependence. In this doping range the B band is far from its own Lifshitz transition, which would take place at a much higher doping inaccessible experimentally $p = 0.33$. Therefore, its contribution to the Raman B_{1g} response (dot-dashed curves in Fig. 8) is less relevant than the AB band one around $p = 0.22$.

For the sake of completeness in Fig.9 we show the calculated ratio of the integrated Raman intensities $I_{B_{1g}}/I_{B_{2g}}$ (defined in main text) of the AB and B bands separately, as well as the total for a doping range larger than what is accessible experimentally.

Two peaks are clearly discernable, both in the normal and the superconducting cases, at $p = 0.22$ and 0.33 , the first corresponding to the AB band Lifshitz transition, the second to the B band Lifshitz transition. To clarify this latter statement, we also plot the $I_{B_{1g}}/I_{B_{2g}}$ for the AB and B bands separately, which shows each band contributions to the at the Lifshitz transition points. In particular, as we previously stated, the B band contribution to the Raman response at $p = 0.22$ doping is substantially smaller than the AB band one (while the converse is true at $p = 0.33$). The topology of the Fermi

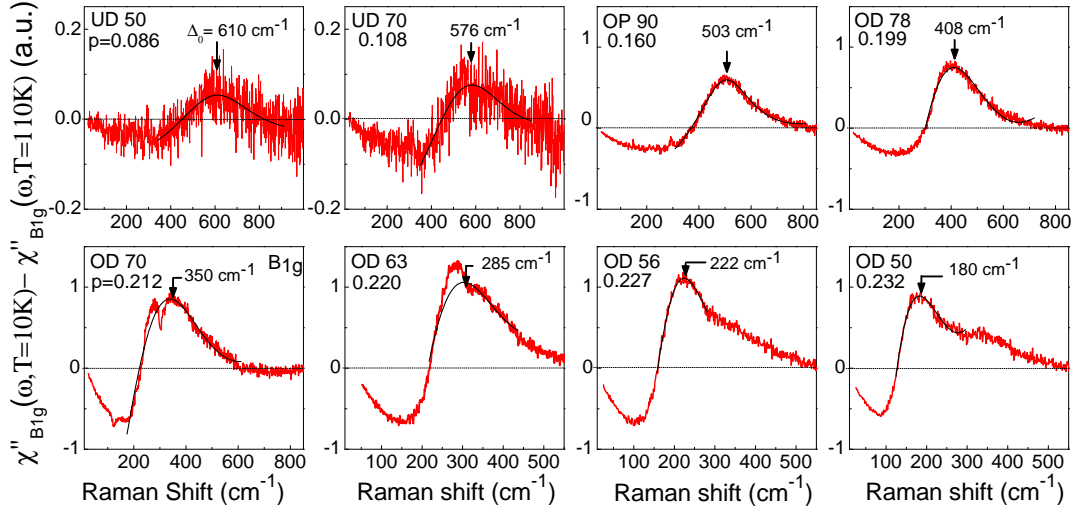


FIG. 5. Subtraction between the normal and superconducting B_{1g} Raman responses of Bi-2212 extracted from fig.1 of the main text. The arrows indicate the location of $2\Delta_0$ in wavenumbers. An accurate estimate of $2\Delta_0$ for OD 70 and OD 63 compounds has been obtained using the 647.1 nm laser line. Indeed, for this excitation line, the phonon peak at 283 cm^{-1} is no more Raman active and does not hamper anymore the estimate of $2\Delta_0$.

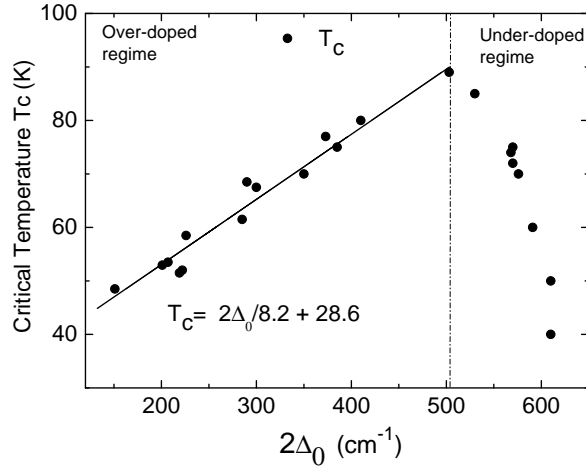


FIG. 6. Evolution of the critical temperature T_c versus pair breaking peak $2\Delta_0$. T_c and $2\Delta_0$ are respectively deduced from magnetic susceptibility and Raman measurements of Bi-2212 crystals with distinct oxygen annealing treatments (see experimental procedure of the main text). The black solid line corresponds to the linear fit of T_c in the overdoped regime. The dashed-dotted line marks off the end of the overdoped regime. The maximum value of T_c is reached for 90 K which corresponds to $2\Delta_0 = 503 \text{ cm}^{-1}$.

surfaces (hole- or electron-like) is also displayed in the top panel for different doping levels, clearly showing the crossing from an hole- to electron-like Fermi surface in the AB and B bands, for $p = 0.22$ and 0.33 .

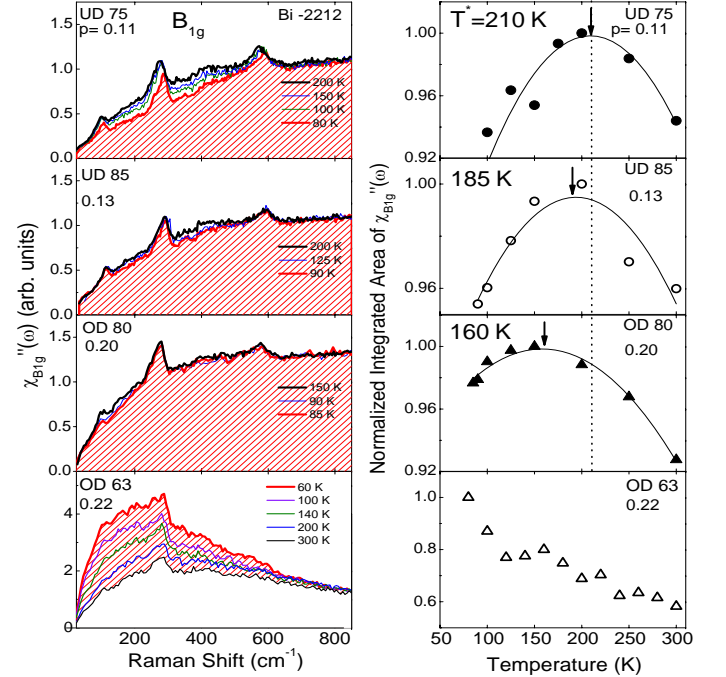


FIG. 7. Left panel: Selected temperature dependences of the B_{1g} Raman spectra of Bi-2212 single crystals for several doping levels. Thick lines underline the low energy electronic background depletion. The area streaked in red corresponds to the electronic background just above T_c . Right panel: Normalized integrated area for the B_{1g} Raman spectra as a function of temperature for distinct levels of doping. Normalization was achieved by dividing the integrated area by its maximum value (up to 800 cm^{-1}). The dotted line is the guide of the eyes and point the value of T^* for $p = 0.115$. The arrows indicate the T^* values for the other doping levels and the thin line corresponds to a polynomial fit. In the bottom right panel the monotonic temperature dependence signifies absence of pseudogap depletion, and T^* is undefined.

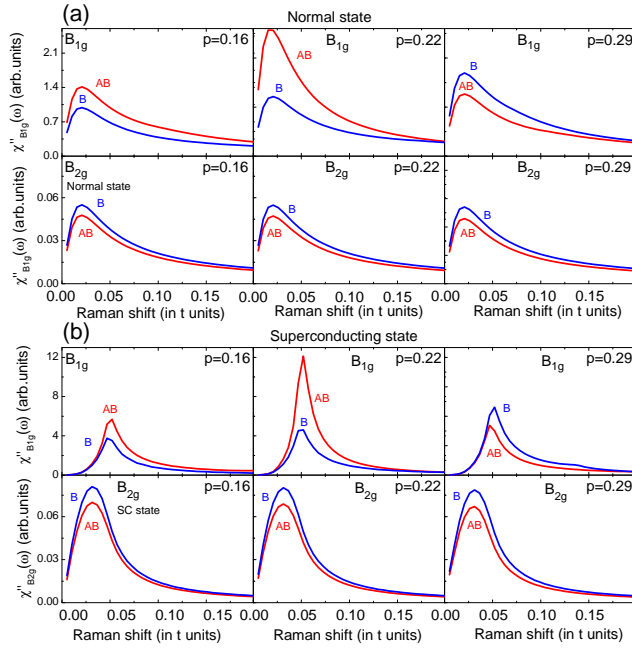


FIG. 8. Raman response evolution (a) in the normal state and (b) superconducting state for three characteristic dopings. The doping level $p = 0.22$ corresponds to a Lifshitz transition where the hole-like AB band becomes electron-like. The AB band contribution is represented by continuous lines, the B band contribution by dot-dashed lines. Both in the normal and the superconducting states the B_{1g} response of the AB band shows a substantial enhancement at the van Hove singularity associated with its Lifshitz transition. The B_{2g} response, by contrast, is only weakly doping dependent.

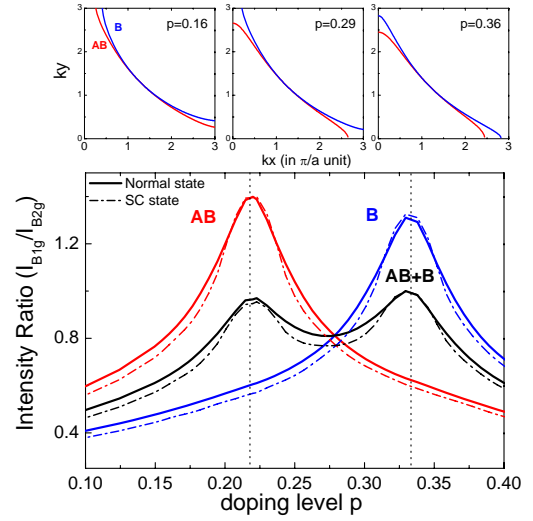


FIG. 9. Integrated intensity ratios $I_{B_{1g}}/I_{B_{2g}}$ for the normal (solid lines) and superconducting (dash-dot lines) phases over a doping range wider than what is accessible experimentally. The contributions from the AB (red) and B (blue) bands are shown separately. They peak at $p = 0.22$ and 0.33 respectively, which correspond to the Lifshitz transitions in each of these bands, as shown in the top panel. Note that around $p = 0.22$ the AB band contribution is dominant. The physical intensity ratios obtained from the total responses, i.e., the sum of the responses from the two bands, is shown in black. All the curves for a given phase are normalized by the value of the total response in that phase at $p = 0.22$.

-
- [1] Presland, M.R., Tallon, J.L., Buckley, R.G., Liu, R.S. & Flower, N.E. General trends in oxygen stoichiometry effects on T_c in Bi and Tl superconductors. *Physica C* **176**, 95-105 (1991).
- [2] Sacuto A. *et al.* New insights into the phase diagram of the copper oxide superconductors from electronic Raman scattering. *Rep. Prog. Phys.* **76**, 022502 (2013).
- [3] Devereaux, T.P. & Hackl, R. Inelastic light scattering from correlated electrons. *Rev. Mod. Phys.* **79**, 175 (2007).
- [4] Chubukov, A.V. & Norman, M.R. One-gap scenario to explain Raman scattering in a d-wave superconductor. *Phys. Rev. B* **7**, 214529 (2008).